Self-Assembled Morphologies of a Diblock Copolymer Melt Confined in a Cylindrical Nanopore

Weihua Li[†] and Robert A. Wickham*

Department of Physics, St. Francis Xavier University, Antigonish, Nova Scotia, Canada B2G 2W5

Received July 19, 2006; Revised Manuscript Received September 19, 2006

ABSTRACT: We systematically investigate the microdomain morphologies that self-assemble in a diblock copolymer melt confined to a narrow cylindrical nanopore using real-space self-consistent mean-field theory. We observe, for a bulk cylinder-forming copolymer, that a variety of novel microdomain structures emerge under confinement. As the pore diameter increases, the following sequence of stable structures occurs: single cylinder, stacked disks, single helix, double helix, toroid−sphere, and helix−cylinder. We accurately locate the pore diameters where first-order phase transitions between these morphologies occur. We vary the interaction of the diblock copolymer with the pore wall from being preferential for the minority block to neutral to being preferential for the majority block and find that the sequence of structures is unchanged, for these interactions. The pitch angle of the helices and the pore diameter can be related using a simple geometrical argument. Over the range of pore diameters we examine, phases involving arrangements of multiple straight cylinders along the pore axis have significantly higher free energy than the structures mentioned above. Our results are consistent with experiments and a recent simulated annealing study.

I. Introduction

Macromolecular self-assembly has attracted much interest as an efficient and effective means to create structures at nanometer scales. Potential applications for these structures include lithographic templates for nanowires, photonic crystals, and high-density magnetic storage media.[1] Confinement effects, produced by boundaries, influence the self-assembly process and can generate novel mesostructures, with potentially novel applications. Confined diblock copolymer melts have become the focus of increasing study. In the bulk, these materials form a variety of periodic mesostructures—lamellae, hexagonally coordinated cylinders, body-centered-cubic lattices of spheres, and the gyroid morphology. The ability to tune the period and to control self-assembly using temperature, chemical composition, and molecular architecture lend a rich physics to these materials and make them attractive for industrial applications.[1−4] Competition between the chain stretching energy and the interfacial energy between block domains determines which structures form in the bulk. Introducing confinement modifies this competition. Confinement of diblock copolymers between parallel solid walls, or in a thin film, has been extensively studied.[5−9] Relative to this, the effect of confinement in a cylindrical pore on the self-assembly process is far less explored and is now attracting significant interest.

Recent experimental studies by Russell's group of asymmetric and symmetric polystyrene-*b*-polybutadiene (PS-*b*-PBD) diblock copolymers confined to relatively wide (greater than 100 nm diameter) cylindrical nanopores in alumina observed straight cylindrical and concentric lamellar domains in the pore.[10] Concentric lamellae were also seen in symmetric polystyrene-*b*-poly(methyl methacrylate) diblock copolymers confined in alumina nanopores of similar diameter.[11] Concentric lamellar structures have been observed in Monte Carlo simulations[12] and dynamic density functional simulations.[13] Both straight cylinders and concentric lamellae are translationally invariant along the pore axis and are thus effectively two-dimensional structures. In our recent work, we applied self-consistent mean-field theory (SCMFT) to systematically evaluate the phase diagram for two-dimensional structures that form under confinement in relatively wide cylindrical pores.[14] We discovered a rich variety of new structures, including the experimentally observed straight cylindrical and concentric lamellar domains. We expect, however, that some of the two-dimensional structures we observed will be unstable to undulations along the axial direction that would relax the stress associated with confinement by the pore walls. In fact, fully three-dimensional microdomains, including stacked disks, helices, and lines of spheres, were observed by Russell's group in narrower (less than 50 nm diameter) pores.[15−17] Various three-dimensional mesostructures, including helices and stacked toroids, were observed to self-assemble in a silica−surfactant composite confined in narrow (less than 100 nm diameter) cylindrical nanopores.[18] A SCMFT calculation for a homopolymer−diblock copolymer blend that accompanied the silica−surfactant experiment supported the existence of such three-dimensional structures under confinement.[18]

A complete physical picture for these confined three-dimensional structures, explaining the conditions under which they will appear, the extent of their stability, the transition points between phases, and their mechanism of formation does not yet exist. For example, helical domain structures are also found in SCMFT calculations of binary blends of symmetric diblock copolymer subjected to an extensional force field.[19] Helical and catenoid-cylinder structures have been observed to form in Monte Carlo simulations of symmetric diblock copolymers, depending on the strength of the preference of the pore wall for either block.[20,21] The mechanism for helix formation under these conditions is not fully understood. Our previous work revealed a rather complex phase diagram which suggests that a wide variety of confined three-dimensional structures may exist.[14] If such diversity exists, then it follows that these confined systems would potentially have a wider range of application. However, understanding the formation of three-dimensional

[†] Present address: Department of Physics and Astronomy, McMaster University, Hamilton, Ontario, Canada L8S 4M1. E-mail: wli@mcmaster.ca.
* Corresponding author. E-mail: rwickham@stfx.ca.

10.1021/ma061630+ CCC: $33.50
Published on Web 10/28/2006

structures will require subtle physical arguments. A step toward a better theoretical understanding was taken in a recent simulated annealing study that systematically examined the structures that form when an asymmetric diblock copolymer melt is confined in a narrow pore.[22] This simulation found a variety of interesting three-dimensional mesophases as the pore diameter and the interaction between the copolymer and pore wall were varied.

To date, SCMFT has not been applied to the problem of the formation of three-dimensional microdomains in a diblock copolymer melt confined in a cylindrical nanopore. Here, we extend our previous SCMFT study into the third dimension and systematically examine microstructure formation in narrow pores. SCMFT has proved to be one of the most successful theoretical methods for investigating equilibrium phases in block copolymers and has played a major role in establishing and understanding the phase diagram of the bulk diblock copolymer melt.[23,24] We focus here not on the effect of molecular parameters but on the environment, that is, the pore size and the interaction of the copolymer with the pore wall. Thus, our focus is similar to that of ref 22, and we will closely compare our results to theirs. Our SCMFT approach, however, has the significant advantage over the simulated annealing technique in ref 22 that the free energy of the microphases can be computed, allowing for comparison of the relative stability of the phases. The present work and ref 22 are thus complementary. Furthermore, detailed, accurate information about the domain structure, polymer configurations, and chain stretching can be provided by SCMFT, making this technique ideally suited to address, for example, the question of the formation mechanism for these structures. We observe a variety of novel three-dimensional microphases that have no analogue in the unconfined system. The resolution of our study enables us to accurately locate the phase boundaries and phase stability regions as the pore diameter is varied.

II. Theory

A. Self-Consistent Mean-Field Theory. We consider an incompressible melt of AB diblock copolymers, confined to a cylindrical pore of radius R (diameter $D = 2R$). Each copolymer has a degree of polymerization N while the A block on each has a degree of polymerization fN with $0 \le f \le 1$. Lengths in our theory are expressed in units of the radius of gyration, $R_g = a\sqrt{N/6}$, of the copolymer. The statistical segment length is a. Within the mean-field approximation to the many-chain Edwards theory,[25,26] at a temperature T the free energy F for n Gaussian diblock copolymer chains confined in a cylindrical pore has the form

$$\frac{F}{nk_BT} = -\ln Q + \frac{1}{V}\int_{|\mathbf{r}|\le R} d\mathbf{r}\, \{\chi N \phi_A(\mathbf{r})\, \phi_B(\mathbf{r}) - \omega_A(\mathbf{r})\, \phi_A(\mathbf{r}) - \omega_B(\mathbf{r})\, \phi_B(\mathbf{r}) + H(\mathbf{r})[\phi_A(\mathbf{r}) - \phi_B(\mathbf{r})]\} \quad (1)$$

The monomer densities are ϕ_A and ϕ_B; the partition function Q is for a single polymer interacting with the mean fields ω_A and ω_B produced by the surrounding chains. These quantities have the standard definitions and meanings.[23,24] The Flory−Huggins interaction parameter, χ, characterizes the repulsion between dissimilar monomers. In the confined melt, the spatial integration is restricted to the pore volume, taken to be V.

We examine three scenarios for the interaction of the polymer with the pore wall: (a) the pore wall prefers the majority B block, (b) the pore wall prefers the minority A block (we will fix $f = 0.2$ below), and (c) the pore wall is nonpreferential or neutral. We achieve this by introducing a short-range surface field $H(\mathbf{r})$ in eq 1. For convenience, this surface field is chosen to have the form

$$\frac{H(\mathbf{r})}{\chi N} = \beta\{\exp[(|\mathbf{r}| - R)/\lambda] - e^{-\sigma/\lambda}\} \quad (2)$$

for $R - \sigma \le |\mathbf{r}| \le R$, while $H(\mathbf{r}) = 0$ for $|\mathbf{r}| < R - \sigma$. We choose the cutoff distance for the surface interaction to be $\sigma = R_g$, and the decay length to be $\lambda = 0.5R_g$. We take $\beta = +1$ if the pore wall prefers the B block, $\beta = -1$ if the pore wall prefers the A block, and $\beta = 0$ if the pore wall is neutral. With these choices, the interaction between the blocks and the pore wall is comparable (for $\beta \neq 0$) to the interaction between the blocks themselves.

Minimization of the free energy with respect to the monomer densities and mean fields leads to the set of mean-field equations

$$\omega_A(\mathbf{r}) = \chi N \phi_B(\mathbf{r}) + H(\mathbf{r}) + \eta(\mathbf{r}) \quad (3)$$

$$\omega_B(\mathbf{r}) = \chi N \phi_A(\mathbf{r}) - H(\mathbf{r}) + \eta(\mathbf{r}) \quad (4)$$

$$\phi_A(\mathbf{r}) = \frac{1}{Q}\int_0^f ds\, q(\mathbf{r},s)\, q^\dagger(\mathbf{r},s) \quad (5)$$

$$\phi_B(\mathbf{r}) = \frac{1}{Q}\int_f^1 ds\, q(\mathbf{r},s)\, q^\dagger(\mathbf{r},s) \quad (6)$$

with

$$Q = \frac{1}{V}\int_{|\mathbf{r}|\le R} d\mathbf{r}\, q(\mathbf{r},s)\, q^\dagger(\mathbf{r},s) \quad (7)$$

Incompressibility

$$\phi_A(\mathbf{r}) + \phi_B(\mathbf{r}) = 1 \quad (8)$$

is enforced via the Lagrange multiplier $\eta(\mathbf{r})$, for $|\mathbf{r}| < R$. A key quantity appearing in these equations is the end-segment distribution function $q(\mathbf{r},s)$, which is proportional to the probability that a polymer chain segment, of contour length s and with one free end, has its other end located at $\mathbf{r}$. Both this distribution function and its conjugate, $q^\dagger(\mathbf{r},s)$, satisfy the modified diffusion equations

$$\frac{\partial q(\mathbf{r},s)}{\partial s} = \nabla^2 q(\mathbf{r},s) - \omega(\mathbf{r},s)\, q(\mathbf{r},s) \quad (9)$$

$$-\frac{\partial q^\dagger(\mathbf{r},s)}{\partial s} = \nabla^2 q^\dagger(\mathbf{r},s) - \omega(\mathbf{r},s)\, q^\dagger(\mathbf{r},s) \quad (10)$$

with $\omega(\mathbf{r},s) = \omega_A(\mathbf{r})$ for $0 \le s \le f$ and $\omega(\mathbf{r},s) = \omega_B(\mathbf{r})$ for $f < s \le 1$. The initial conditions are $q(\mathbf{r},0) = 1$ and $q^\dagger(\mathbf{r},1) = 1$. Equations 3−10 can be solved self-consistently in real space to find the equilibrium densities.[23,24,27] We align the pore axis with the z-axis; the cross section of the pore is in the $x-y$ plane. We employ a parallel version[28] of the split-step Fourier method of Tzeremes et al.[29] to solve the modified diffusion equations for the end-segment distribution functions on a $N_x \times N_y \times N_z = 128 \times 128 \times 64$ cubic lattice. This lattice is divided between up to eight processors. A range of pore diameters is examined, and the periodicity of the structure along the pore axis is adjusted to minimize the free energy; thus, the lattice spacings, Δx, Δy, and Δz also vary. Typical values are $\Delta x = \Delta y \approx (0.1-0.2)R_g$ and $\Delta z \approx 0.1R_g$. The chain contour length for each block is discretized into 64 segments. Our previous work in two dimensions with wider pores suggested that the stability regions

and phase boundaries are not significantly altered if we use a finer mesh than $N_x \times N_y = 128 \times 128$.[14] In the current system we find that the free energy of the system is insensitive to variations in N_z from 64 to 128 to 256, suggesting that our $128 \times 128 \times 64$ lattice is sufficiently large to produce an accurate phase diagram for the range of D we examine.[30] Outside the pore there is no polymer, so we set the end-segment distribution functions to zero when $x^2 + y^2 \geq R^2$, which implies that $\phi_A = \phi_B = 0$ in this region.[31] In the $x-y$ plane, the lattice size is slightly larger than the diameter of the cylindrical pore. We impose periodic boundary conditions on all edges of the lattice. Since the monomer densities and end-segment distributions are zero outside the cylinder, we expect, as demonstrated in our previous work,[14] that the periodic images of the pore will not influence the behavior in the pore.

We first use random initial conditions for the mean fields in our iterative algorithm to generate a diverse set of solutions to the mean-field equations over a range of pore diameters. We find that it is difficult to find helical structures as solutions to the mean-field equations unless the initial condition in the iterative procedure is chiral. We introduce chirality into our initial conditions by randomly initializing the mean fields on a slice in the $x-y$ plane and then relating the mean fields at other z values to the mean fields on this slice through a translation along z and a rotation (a screw transformation). A right-handed screw can iterate to a right-handed helical structure, and a left-handed screw can iterate to a left-handed one. Once we determine a set of solutions to the mean-field equations, we then use these solutions as initial conditions in our algorithm to explore the extent (if any) of their stability regions. As noted above, for a given structure we adjust its period along the z-axis so as to minimize its free energy. We compute free energies to an accuracy of 1 part in 10^{-4}. We take the equilibrium phase to be the structure which has the lowest free energy, for a given f, χN, and D, of all the structures we observe. This is a reasonable and necessary approach to construct the phase diagram since a method does not currently exist, within SCMFT, to directly identify the global minimum of the free energy.

B. Relation between the Helical Pitch Angle and the Pore Diameter in the Strong Segregation Limit. Some of the structures that we find below have the property that their monomer density cross section in the $x-y$ plane does not depend on z, up to a rotation. The helical microdomain is an example. For such structures, in the strong-segregation limit, the copolymer composition enforces the condition

$$A = \frac{\pi D^2}{4} f \tag{11}$$

on A, defined as the area, in the $x-y$ plane, that is minority phase (we take $f < 0.5$ for definiteness). We define the pitch angle, α, of a helical structure to be the angle that the axis of the helix makes with the $x-y$ plane. For a structure composed of m helices with a pitch angle α and with a cross-sectional area perpendicular to the helix of A_0 per helix, simple geometrical projection yields the relation

$$\sin \alpha = \frac{mA_0}{A} \tag{12}$$

which holds approximately, for sufficiently large α.[32] Equations 11 and 12 lead to the following approximate relation between pitch angle and pore diameter:

$$\sin \alpha = \frac{4mA_0}{\pi D^2 f} \tag{13}$$

If we assume that the helices are free to adjust A_0 to an optimal value which is independent of D, then eq 13 suggests $\sin \alpha \sim D^{-2}$.

III. Results and Discussion

We fix $f = 0.2$ and $\chi N = 40$. In the bulk, such a diblock copolymer forms hexagonally coordinated cylindrical microdomains of the minority A species with a spacing of $L_0 \approx 4.30 R_g$ between the centers of the cylinders.[33] This work examines new morphologies that emerge under confinement, as the pore diameter is varied. We study narrow pores, with diameters of only a few L_0, since three-dimensional structures were observed experimentally for such pore sizes.[16,17]

Figure 1 displays the equilibrium microstructures we find as the pore diameter D varies, subject to the three pore wall interactions we examine. This is the main result of this paper. The sequence of structures we observe, as D increases, is independent of the pore wall interactions, for the interactions we examine. The sequence is: a single cylindrical microdomain (C_1), stacked disks of the minority phase (Dk), a single helix (H_1), a double helix (H_2), stacked toroids alternating with spheres (TS), a single helix winding around a central cylinder (H_1C), a double helix winding around a central cylinder (H_2C). Our preliminary examination of narrower pores (e.g., $D/L_0 \approx 0.2$) suggests that C_1 will break up into a line of beadlike microdomains, if the pore is narrow enough. Experiments,[17,18] a SCMFT study of a homopolymer/copolymer blend,[18] and a simulated annealing study[22] observed beadlike microdomains in very narrow pores, consistent with our results. In pores wider than those shown in Figure 1 the morphologies become more complicated, and the free energy differences between structures become very small, making it difficult to determine which structure is stable. In fact, we have not been able to determine the relative stability of H_1C and H_2C in this work, although we believe the sequence is H_1C to H_2C, in analogy with H_1 to H_2. For this reason the transition between H_1C and H_2C is not indicated in Figure 1.

A. Influence of the Pore Wall Interaction on the Microstructures. Phase transitions occur at similar values of D/L_0 when the pore wall is neutral as when the pore wall prefers the B block (Figure 1a,c). In both cases the majority B block is near the wall (when the pore wall is neutral this occurs for entropic reasons). Thus, it is not surprising that the self-assembly process in the interior of the pore is similar for the two cases. The transition between H_1 and H_2 is an exception, and its location is sensitive to the pore wall interaction, suggesting that this interaction plays a significant role in determining the relative stability of these helical phases. The combined size of the H_1 and H_2 stability regions, however, appears insensitive to the pore wall interaction, for the three cases we examine.

When the pore wall attracts the minority A species, the pore diameters at which phase transitions occur increase by $\sim 1.5L_0$, compared to the other two cases. A thin layer of the A block forms near the pore wall (Figure 1b), with the associated B block on the inside of the curvature of the AB interface. Thus, the middle of the pore, inside this B block, is an effectively narrower pore, with "walls" that are preferential for B. The physics of self-assembly then proceeds as in the other two cases. The value of $1.5L_0$ suggests that the chains near the pore wall are stretched compared to the bulk. This is expected since the majority B block is forced to be on the inside of the curvature. This effect

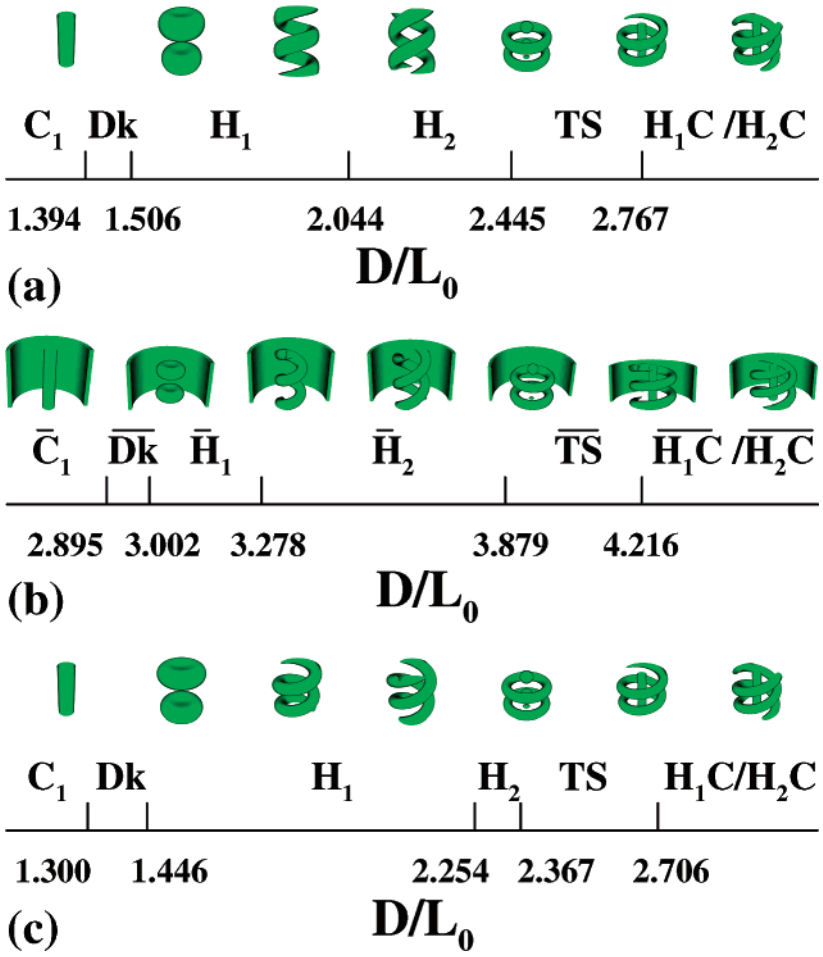

Figure 1. Phase diagram for a diblock copolymer melt, with $f = 0.2$ and $\chi N = 40$, confined in cylindrical pores of various diameters, D, measured in units of the center-to-center distance, L_0, between cylinders in the bulk. Three scenarios for the polymer/pore wall interaction are shown: (a) the pore wall prefers the majority B block, (b) the pore wall prefers the minority A block, and (c) the pore wall is nonpreferential or neutral. The phases are labeled C_1 for a single straight cylinder, *Dk* for stacked disks, H_1 for single helix, H_2 for double helix, *TS* for alternating toroids and spheres, and H_1C and H_2C for a single and double helix, respectively, surrounding a central straight cylinder. Their regions of stability and phase boundaries are indicated. An overbar on the phase label indicates that the structure is enclosed by a thin layer of the A domain. Representative morphologies are indicated above the symbol; the $\phi_A(\mathbf{r}) = 0.5$ surface, containing the minority phase, is shown.

was also observed in our two-dimensional study[14] and in the simulation of ref 22.

B. Sequence of Microstructures with Increasing Pore Diameter. We now focus on understanding the sequence of microstructures we observe as the pore diameter increases. The C_1 structure has a constant-curvature AB interface and azimuthally uniform chain stretching. In the bulk, at a fixed χN and f, the cylindrical minority domain will assume a diameter that minimizes the free energy.[34] In the confined melt, this should lead, based on eq 11, to a pore diameter that is optimal for the formation of C_1. When D increases beyond this, C_1 will become unfavorable since entropy is lost by chain stretching. The *Dk* phase which forms can allow the system to relax this stretching since the system is free to adjust the stacking period along the pore axis. The stacking period is insensitive to the type of polymer/pore wall interaction and varies from $0.88L_0$ to $0.93L_0$ over the region of stability of *Dk*. The nearly flat AB interfaces forming the faces of the disks are unfavorable for a cylinder-forming copolymer. With increasing pore diameter these faces widen and the *Dk* phase becomes metastable with respect to the single helix phase, H_1. This sequence of first-order transitions is shown in Figure 2, where we plot of free energy of the C_1, *Dk*, and H_1 phases as a function of the pore diameter, for the case where the pore wall prefers the majority B block.

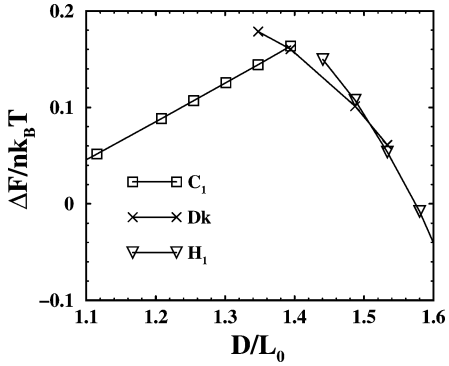

Figure 2. Free energy per polymer, in units of k_BT, of the C_1 (squares), *Dk* (×), and H_1 (inverted triangles) phases as a function of the pore diameter D, measured in units of the center-to-center distance, L_0, between cylinders in the bulk. The pore wall prefers the majority B block. To highlight the region where the curves cross, we subtract a linear function from all the scaled free energies, F/nk_BT, and plot $\Delta F/nk_BT = F/nk_BT - [0.625D/L_0 - 1.85]$.

On the basis of the argument that constant curvature AB interfaces are favorable,[24] the H_2 phase should actually be favored over H_1, since we find (not shown) that the cross section of the minority, helical domain in the H_2 phase is closer to being circular than that in the H_1 phase. However, eq 11 imposes a

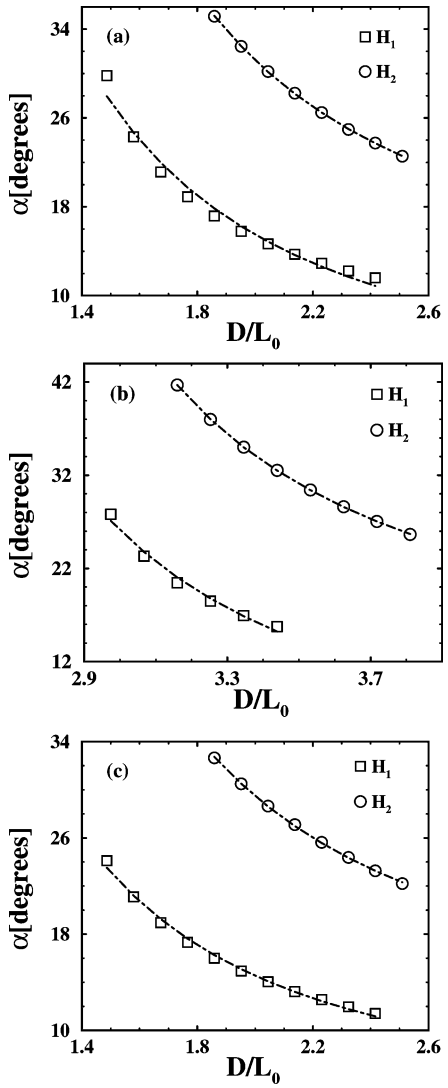

Figure 3. Pitch angle, α, of the H_1 (squares) and H_2 (circles) structures as a function of the pore diameter D, measured in units of the center-to-center distance, L_0, between cylinders in the bulk. In (a) the pore wall prefers the majority B block, in (b) the pore wall prefers the minority A block, and in (c) the pore wall is neutral. The pitch angle is defined as the angle that the axis of the helix makes with the plane perpendicular to the pore axis. The data include the pitch angle for both stable and metastable H_1 and H_2 structures. The dot−dashed lines are fits to eq 14 or, in (b), eq 14 with $D \rightarrow D - 1.5L_0$.

constraint that may force the diameter of the minority domain to be smaller than optimal if the H_2 phase were to exist in narrower pores. This suggests why the H_1 phase appears first in narrower pores.

The pitch angle of both H_1 and H_2 is a decreasing function of the pore diameter, as we show in Figure 3. Motivated by eq 13, we find that the formula

$$\sin \alpha = c_0\left(\frac{L_0}{D}\right)^2 + c_1 \qquad (14)$$

where c_0 and c_1 are adjustable fit parameters, produces excellent fits to our data, which are also shown in Figure 3. Note that when the pore wall prefers the minority phase (Figure 3b) we have adjusted $D \rightarrow D - 1.5L_0$ in eq 14 to account for the narrower effective pore. The fitted values of c_0 and c_1 are given in Table 1. Equation 13 itself produces poorer fits to our data than eq 14. This is true whether we fix A_0 in eq 13 to take the value for bulk cylinders in the strong-segregation limit, $A_0 = \sqrt{3}L_0^2 f/2$ (equivalently, $c_0 = 2\sqrt{3}m/\pi$ and $c_1 = 0$ in eq 14), or whether we allow A_0 to be an adjustable fit parameter. This highlights the approximate nature of eq 13 and suggests that A_0 depends slightly on D. Equation 13 does, however, suggest that the pitch angle of the double helix ($m = 2$) should be approximately twice that of the single helix ($m = 1$), as we observe in Figure 3.

Table 1. Parameters Obtained from Fits of the Pitch Angle vs the Pore Diameter in Figure 3 to Eq 14[a]

situation	c_0	c_1
H_1, wall prefers majority	1.00	0.018
H_1, wall prefers minority	0.99	−0.002
H_1, neutral wall	0.731	0.069
H_2, wall prefers majority	1.47	0.15
H_2, wall prefers minority	1.32	0.19
H_2, neutral wall	1.23	0.18

[a] A simple strong-segregation calculation (see text) gives $c_0 = 2\sqrt{3}m/\pi$ and $c_1 = 0$. Thus, in the strong-segregation calculation, $c_0 \approx 1.10$ for single helices and $c_0 \approx 2.20$ for double helices.

If the pitch period of the helix is too high, the majority B chains can be unfavorably stretched between winds of the helix. The pitch period of H_1 is approximately L_0, varying from slightly greater than L_0 to slightly less than L_0 with increasing D over the H_1 stability region. This suggests that the *Dk* phase forms where it does as a compromise to reduce the unfavorable chain stretching that occurs in both the C_1 and H_1 phases in this region.

In wider pores, the H_2 phase becomes stable and has a minority helical A domain with a cross section that is close to circular. As we increase the pore diameter, the H_2 structure transforms into the *TS* phase, suggesting that unfavorable chain stretching in the center of the pore in the H_2 phase is relieved by the formation of minority spherical domains along the pore axis in the *TS* phase. The high interfacial curvature of the spheres is unfavorable, and when the pore diameter is slightly larger, the system is able to accommodate a central cylindrical domain along the pore axis. This sphere-to-cylinder transition in the center of the pore seems analogous to the sphere to C_1 transition in narrower pores. The H_1C and H_2C phases that occur can be viewed as analogues of the H_1 and H_2 phases seen in narrower pores.

In addition to the stable structures shown in Figure 1, we observe several metastable structures. While the two-dimensional C_1 phase is stable, we observe that other two-dimensional structures, such as C_3, C_4, C_{1-5}, and C_{1-6} (in the notation of our previous work[14]) have no domain of stability in the parameter region we examine. This suggests that the stress associated with confinement in narrow pores causes these two-dimensional structures to become unstable to density fluctuations along the pore axis. Experiment suggests that such straight cylindrical phases should occur for pore diameters satisfying $D/L_0 > 4$, as the center of the pore approaches an environment more like the bulk.[16] However the value of D/L_0 at which this transition occurs, and its dependence on χN and f, is not yet known from theory. Our present results suggest that some of the two-dimensional phases we identified as stable in our earlier work[14] may actually be metastable. However, in our earlier work we studied wider pores than the ones we examine here (including $D/L_0 > 4$) and studied weaker segregation, leading us to expect that some of the phases we observed in our earlier work are robust, stable two-dimensional phases.

With the exception of the *TS* phase, we find that structures involving stacked toroidal domains, or stacked toroids with cylinders, are metastable. The stable *Dk* phase will sometimes emerge out of a metastable tilted toroid structure as the structural

period along the pore axis is optimized. These results suggest that toroids are unfavorable in these narrow pores due to the high degree of bending of the cylindrical domain making up a toroid.

C. Comparison with Experiments and Simulation. A helical structure was recently observed in experiments using a PS-*b*-PBD melt confined in narrow 33−45 nm ($D/L_0 = 1.1-1.5$) pores in an alumina substrate.[16] The volume fraction of PBD was 0.36, and the pore wall was preferential for PBD. Our results suggest that helices form over the range $D/L_0 \approx 3.0-3.9$ when the pore wall prefers the minority block and over the range $D/L_0 \approx 1.4-2.3$ when the pore wall is neutral. This suggests that the pore wall in ref 16 had a weaker preference for the minority PBD than the value we use here. The helical pitch angle of 18° measured in these experiments is comparable to our results for H_1, for the case of a neutral wall (Figure 3c).

Earlier experimental work with silica−surfactant composite mesostructures confined in nanoporous alumina observed structures similar to those we observe here at various pore diameters.[18] In a 31 nm pore, they observed a double helix (H_2), while in wider, 34−45 nm pores they observed a central straight cylinder surrounded by either stacked toroids (50% of cases), a single helix (H_1C) (44% of cases), or a double helix (H_2C) (6% of cases). We also see that H_2 forms in narrower pores and that H_1C and H_2C form in wider pores, although we find structures involving stacked toroids are metastable. Consistent with our results, they found more complex morphologies form in even wider pores, and they did not observe structures involving multiple straight cylinders. Their SCMFT calculation, for a diblock copolymer/homopolymer blend (30% homopolymer by volume), found several solutions to the mean-field equations that suggested the sequence C_1, H_1, H_2, H_2C with increasing pore diameter. This is similar to the sequence we observe for the neat diblock copolymer melt, although neither the experiment nor their SCMFT calculations reported observing the *Dk* or *TS* structures that we see. These phases simply may have been missed in ref 18 while our study finds them since we are able to accurately locate the phase boundaries due to our investigation of closely spaced D/L_0 values and our comparison of the free energies. An interesting alternative explanation is that it is not necessary to form intermediate *Dk* or *TS* morphologies in the silica−surfactant (homopolymer/copolymer blend) system since the silica (homopolymer) acts as a filler and is able to position itself to alleviate the free energy penalty associated with chain stretching in the C_1 and H_1 (or H_2 and H_1C) phases. This should lower the free energy of these phases and may allow for direct C_1-to-H_1 and H_2-to-H_1C transitions in the silica−surfactant (blend) system (see Figure 2). This mechanism may also explain why toroids are seen in the silica−surfactant system but are only metastable in our SCMFT study of the neat diblock copolymer.

Very recently, Yu et. al. systematically studied the present problem using a simulated annealing Monte Carlo technique.[22] Our SCMFT results in Figure 1 correlate with Figure 1 of ref 22. When the pore wall prefers either the majority or minority block, the sequence of phases we observe and our values of D/L_0 at the phase boundaries are in excellent agreement with ref 22. This agreement suggests that the positions of the phase transitions are not highly sensitive to the values of f and χN since ref 22 studied $f = 1/6$, for these cases, and likely worked at a stronger segregation and a different pore wall interaction than in our study. We can compute the free energies and relative stabilities of our phases, and we can use our results to suggest which structures seen in the simulated annealing study are metastable. For example, when $D/L_0 = 2.1$ and the pore wall prefers the majority block ref 22 observed that H_1, H_2, and stacked toroids were degenerate structures. Our results indicate that H_2 is stable at this value of D/L_0, with H_1 being stable in narrower pores, and that stacked toroids are metastable. Furthermore, our results suggest that the tilted disks seen in ref 22 are metastable with respect to the *Dk* phase. Our observation that the free energy differences between structures become very small in wider pores ($D/L_0 \gtrsim \sim 3$) may explain why the authors of ref 22 stated they observed structures "plagued with defects" in this region. There are differences between the results ref 22 and our results in the case of a neutral pore wall. Notably, phases with multiple straight cylinders were seen in ref 22, while our study finds these phases to be clearly metastable compared to the structures we show in Figure 1c. This suggests that the simulated annealing study is having difficulty equilibrating when the pore wall is neutral. At the intermediate segregation that both we and ref 22 examine, we do not expect composition fluctuations, which are included in the simulated annealing study but are not included in SCMFT, to play a significant role.[35] Since we can identify metastable structures, our present SCMFT study is a necessary complement to the simulated annealing study.

The discussion above suggests that structures like C_1, H_1, H_2, H_1C, and H_2C constitute a common structural motif in a variety of contexts: this work, simulated annealing studies,[22] and two experiments involving different materials.[16,18] On the other hand, the existence of the *Dk* and *TS* phases that we observe here, and also the existence of the phases involving stacked toroids in ref 18 appears to depend on the specific details of the system. We speculate that the generic nature of the C_1, H_1, H_2, H_1C, and H_2C phases may be due to the constraint, eq 11, imposed by geometry and composition, that these structures must satisfy. Furthermore, we should note that we observe the *Dk* and *TS* phases when L_0 is incommensurate with the (effective) pore diameter: $D/L_0 \approx (k + 1/2)$ where k is an integer. For these pore diameters the system is most likely to form morphologies with complicated monomer density variations along the pore axis, which do not have to satisfy eq 11.

IV. Conclusions

In summary, we have extensively and systematically employed real-space SCMFT to explore the three-dimensional microstructures that form when a diblock copolymer melt is confined to relatively narrow cylindrical nanopores of various diameters. We have identified a sequence of novel structures, not seen in the bulk, that form with increasing pore diameter. The sequence of structures we found was insensitive to the pore wall interaction, for the three pore wall interactions we examined. We accurately located the first-order phase boundaries between the stability regions of the various microstructures. Interestingly, chiral structures, such as single and double helices can arise, despite the fact that our model involves achiral molecules. This has precedent—chiral self-assembly from achiral building blocks was also observed experimentally as a helical morphology in neat ABC triblock copolymers by Krappe et al.[36] We found that the pitch angle of the helical structures and the pore diameter satisfy a relationship that can be motivated from a simple geometrical argument. Our results are consistent with experiments. Our results are also consistent with a recent simulated annealing study but suggest that some of the structures seen in this study are metastable. When viewed along with experiment and simulation, our results suggest that the phases C_1, H_1, H_2, H_1C, and H_2C are robust, while the existence of structures like *Dk* and *TS* may be system-specific. We observed

multiple straight cylinder solutions to be metastable in the range of pore diameters we examined. This suggests that it may be difficult to form straight nanowire templates using narrow nanopores as a confinement mechanism. The diameter at which there is a crossover to bulk behavior in the interior of the pore remains to be determined. Now that we have accurately located the phase boundaries in this system, we can begin to address the issue of the mechanism of structural phase transitions as the pore diameter increases. These transitions appear to result from a combination of effects which need to be quantified.

Acknowledgment. The authors gratefully acknowledge helpful discussions with Professors A.-C. Shi, B. Li, and T. Lodge. The authors also thank the StFX hpcLAB and G. Lukeman for computing resources and support. This work was supported by NSERC and CFI. W. Li gratefully acknowledges support from Professor D. Hunter, and from the NSERC Research Capacity Development in Small Universities program.

References and Notes

(1) Park, C.; Yoon, J.; Thomas, E. L. *Polymer* **2003**, *44*, 6725−6760.
(2) Park, M.; Harrison, C.; Chaikin, P. M.; Register, R. A.; Adamson, D. H. *Science* **1997**, *276*, 1401−1404.
(3) Segalman, R. A.; Yokoyama, H.; Kramer, E. J. *Adv. Mater.* **2001**, *13*, 1152−1155.
(4) Cheng, J. Y.; Mayes, A. M.; Ross, C. A. *Nat. Mater.* **2004**, *3*, 823−828.
(5) Matsen, M. W. *J. Chem. Phys.* **1997**, *106*, 7781−7791.
(6) Morkved, T. L.; Jaeger, H. M. *Europhys. Lett.* **1997**, *40*, 643−648.
(7) Geisinger, T.; Müller, M.; Binder, K. *J. Chem. Phys.* **1999**, *111*, 5241−5250.
(8) Huinink, H. P.; Brokken-Zijp, J. C. M.; van Dijk, M. A.; Sevink, G. J. A. *J. Chem. Phys.* **2000**, *112*, 2452−2462.
(9) Rasmussen, K. Ø. *J. Polym. Sci., Part B: Polym. Phys.* **2004**, *42*, 3695−3700.
(10) Xiang, H.; Shin, K.; Kim T.; Moon, S. I.; McCarthy, T. J.; Russell, T. P. *Macromolecules* **2004**, *37*, 5660−5664.
(11) Sun, Y.; Steinhart, M.; Zschech, D.; Adhikari, R.; Michler, G. H.; Gösele, U. *Macromol. Rapid Commun.* **2005**, *26*, 369−375.
(12) He, X.; Song, M.; Liang, H.; Pan, C. *J. Chem. Phys.* **2001**, *114*, 10510−10513.
(13) Sevink, G. J. A.; Zvelindovsky, A. V.; Fraaije, J. G. E. M.; Huinink, H. P. *J. Chem. Phys.* **2001**, *115*, 8226−8230.
(14) Li, W.; Wickham, R. A.; Garbary, R. A. *Macromolecules* **2006**, *39*, 806−811.
(15) Shin, K.; Xiang, H.; Moon, S. I.; Kim, T.; McCarthy, T. J.; Russell, T. P. *Science* **2004**, *306*, 76.
(16) Xiang, H.; Shin, K.; Kim, T.; Moon, S. I.; McCarthy, T. J.; Russell, T. P. *Macromolecules* **2005**, *38*, 1055−1056.
(17) Xiang, H.; Shin, K.; Kim, T.; Moon, S. I.; McCarthy, T. J.; Russell, T. P. *J. Polym. Sci., Part B: Polym. Phys.* **2005**, *43*, 3377−3383.
(18) Wu, Y.; Cheng, G.; Katsov, K.; Sides, S. W.; Wang, J.; Tang, J.; Fredrickson, G. H.; Moskovits, M.; Stucky, G. D. *Nat. Mater.* **2004**, *3*, 816−822.
(19) Morita, H.; Kawakatsu, T.; Doi, M.; Yamaguchi, D.; Takenaka, M.; Hashimoto, T. *J. Phys. Soc. Jpn.* **2004**, *73*, 1371−1374.
(20) Chen, P.; He, X.; Liang, H. *J. Chem. Phys.* **2006**, *124*, 104906.
(21) Feng, J.; Ruckenstein, E. *Macromolecules* **2006**, *39*, 4899−4906.
(22) Yu, B.; Sun, P.; Chen, T.; Jin, Q.; Ding, D.; Li, B.; Shi, A.-C. *Phys. Rev. Lett.* **2006**, *96*, 138306.
(23) Matsen, M. W.; Schick, M. *Phys. Rev. Lett.* **1994**, *72*, 2660−2663.
(24) Matsen, M. W. *J. Phys.: Condens. Matter* **2002**, *14*, R21−R47.
(25) Helfand, E. *J. Chem. Phys.* **1975**, *62*, 999−1005.
(26) Hong, K. M.; Noolandi, J. *Macromolecules* **1981**, *14*, 727−736.
(27) Drolet, F.; Fredrickson, G. H. *Phys. Rev. Lett.* **1999**, *83*, 4317−4320.
(28) Sides, S. W.; Fredrickson, G. H. *Polymer* **2003**, *44*, 5859−5866.
(29) Tzeremes, G.; Rasmussen, K. Ø.; Lookman, T.; Saxena, A. *Phys. Rev. E* **2002**, *65*, 041806.
(30) In our earlier, two-dimensional, calculation the absolute free energies of the structures were sensitive to the values of N_x and N_y used, but the differences between free energies were only slightly influenced by this discretization.[14] As a consequence, the phase boundaries were not significantly affected.
(31) Operationally, this means that for lattice points closer to the *z*-axis than *R*, incompressibility, eq 8, is enforced. For lattice points at or farther than *R* from the *z*-axis, eq 8 is not satisfied and $\phi_A = \phi_B = q = q^\dagger = 0$ is imposed at these lattice points. We have chosen this approach over other approaches which use incompressibility conditions that smoothly approach zero as the pore wall is approached (ref 5 for example) for simplicity.
(32) The simple eq 12 must break down for small α since the minority domain assumes a toroidal configuration in this limit and *A* must approach a finite value. Equation 12 can also be derived by considering the overall length of the helical domain, subject to the composition constraint (Shi, A.-C., private communication).
(33) This value is obtained from a reciprocal-space SCMFT calculation for the bulk system.
(34) In the bulk, the cylindrical domains do not have exactly circular cross sections, but the deviation from circularity is small.
(35) Fredrickson, G. H.; Helfand, E. *J. Chem. Phys.* **1987**, *87*, 697−705.
(36) Krappe, U.; Stadler, R.; Voigt-Martin, I. *Macromolecules* **1995**, *28*, 4558−4561.

MA061630+